This is the accepted manuscript made available via CHORUS. The article has been published as:

Temperature-dependent ^{29}Si incorporation during deposition of highly enriched ^{28}Si films

K. J. Dwyer, H. S. Kim, D. S. Simons, and J. M. Pomeroy

Phys. Rev. Materials **1**, 064603 — Published 16 November 2017

DOI: 10.1103/PhysRevMaterials.1.064603

Temperature dependent ^{29}Si incorporation during deposition of highly enriched ^{28}Si films

Running title: sticking coefficient of ^{29}Si CVD

Running Authors: Dwyer et al.

K. J. Dwyer

Department of Materials Science and Engineering, University of Maryland, College Park, MD 20740, USA

National Institute of Standards and Technology, Gaithersburg, MD 20899-8423, USA

H. S. Kim

Department of Electrical Engineering, University of Maryland, College Park, MD, 20740, USA

National Institute of Standards and Technology, Gaithersburg, MD 20899-8423, USA

D. S. Simons

National Institute of Standards and Technology, Gaithersburg, MD 20899-8371, USA

J. M. Pomeroy[a)]

National Institute of Standards and Technology, Gaithersburg, MD 20899-8423, USA

[a)]Electronic mail: joshua.pomeroy@nist.gov

In this study, we examine the mechanisms leading to ^{29}Si incorporation into highly enriched ^{28}Si films deposited by hyperthermal ion beams at elevated temperatures in the dilute presence of natural abundance silane (SiH_4) gas. Enriched ^{28}Si is a critical material in the development of quantum information devices because ^{28}Si is free of nuclear spins that cause decoherence in a quantum system. We deposit epitaxial thin films of ^{28}Si enriched *in situ* beyond 99.99998 % ^{28}Si onto Si(100) using an ion beam deposition system and seek to develop the ability to systematically vary the enrichment and measure the impact on quantum coherence. We use secondary ion mass spectrometry to measure the residual ^{29}Si isotope fraction in enriched samples deposited from ≈ 250 °C up to 800

°C. The ^{29}Si isotope fraction is found to increase from < 1 x 10^{-6} at the lower temperatures, up to > 4 x 10^{-6} at around 800 °C. From these data, we estimate the temperature dependence of the incorporation fraction, *s*, of SiH_4, which increases sharply from about 2.9 x 10^{-4} at 500 °C to 2.3 x 10^{-2} at 800 °C. We determine an activation energy of 1.00(8) eV associated with the abrupt increase in incorporation and conclude that below 500 °C, a temperature independent mechanism such as activation from ion collisions with adsorbed SiH_4 molecules is the primary incorporation mechanism. Direct incorporation from the adsorbed state is found to be minimal.

I. INTRODUCTION

In solid state quantum information (QI), enriched ^{28}Si is a critical material for the further development of silicon based quantum computing architectures, e.g., quantum dots, quantum wells, and few dopant atoms in Si. By eliminating ^{29}Si nuclei, which have a non-zero nuclear spin and are present with roughly a 5 % natural abundance, pure ^{28}Si becomes an ideal spin-free environment in which to place the electron and nuclear spins of qubits. Without the randomly fluctuating nuclear spins present, donor spins in ^{28}Si interact with their environment far less than in natural silicon leading to a greatly enhanced coherence time (T_2*). Consequently, ^{28}Si has been dubbed a "semiconductor vacuum"[1]. Theoretical modeling and bulk electron spin resonance (ESR) experiments predicted the enhancement in T_2* to be proportional to the reduction in ^{29}Si concentration[2,3], which further spurred interest in exploiting ^{28}Si experimentally. Numerous research groups have shown through bulk ESR and nuclear magnetic resonance (NMR) experiments of ^{31}P spins in ^{28}Si that nuclear and electron spin

coherence (echoed, T_2) times can easily exceed seconds[1,4–6]. Si and Si/Ge based quantum computing also can benefit from utilization of ^{28}Si, e.g., quantum dots formed in Si and in quantum wells within ^{28}Si/SiGe heterostructures[7,8]. A few of these groups have begun to show both long T_2 times and coherent manipulation in ^{28}Si for both bulk donor spins[9] as well as single electron spins in quantum wells[8] and quantum dots[4,10]. Additionally, qubit manipulation schemes, which have been proposed for arrays of quantum dot qubits, and which involve tuning the qubit ESR frequency via a Stark shift[11], have been demonstrated in single quantum dots in ^{28}Si. This Stark shifting mechanism relies on qubit spins that have very narrow inhomogeneous ESR linewidths of a few kHz[1,12], which have only been shown in a material with homogeneous mass such as highly enriched ^{28}Si.

Despite these advantages, only a limited amount of the most highly enriched ^{28}Si (99.995 % ^{28}Si) is available within the solid state quantum computing community for use in ensemble spin QI experiments. Historically, ^{28}Si has primarily been produced at great cost and effort through international collaborations such as the International Avogadro Coordination (IAC)[13], which produced bulk crystals. Other sources of ^{28}Si include enriched epilayers grown on natural abundance Si substrates, which are more abundant within the community than bulk ^{28}Si but are typically less highly enriched (≈ 99.9 % ^{28}Si). QI experiments on single donor and dot spins largely utilized ^{28}Si epilayer samples and demonstrated the benefit of enriched ^{28}Si to QI. A helpful review of some of the different sources of ^{28}Si that have been used in the QI field has been presented by Itoh and Watanabe[14]. The lack of simply produced, readily available, and consistently highly enriched ^{28}Si has led us to develop a mass selected ion beam deposition system capable of taking natural abundance silane (SiH_4) gas and enriching it *in situ* to an extremely high

level of ^{28}Si just prior to depositing it epitaxially on a target Si(100) substrate. Using this system, thin films of highly enriched materials including ^{28}Si have previously been grown amorphously on Si substrates at room temperature[15,16] as well as epitaxially at higher temperatures (this work). Several other groups have also previously demonstrated enriched ^{28}Si thin film deposition using an ion beam system, though not generally with a focus on high quality material (highly enriched, chemically pure) for QI[17–19].

In addition to the general scarcity of ^{28}Si for semiconductor quantum computing research, a specific need exists for enriched silicon with targeted levels of enrichment to facilitate mapping the dependence of T_2* on ^{29}Si concentration in the few-spin regime. Recent ESR measurements[4,10] of T_2* for single ^{31}P spins in ^{28}Si have disagreed with the theoretical predictions for the same systems[2]. Our ion beam deposition system provides us with a unique opportunity to produce ^{28}Si material at targeted levels of enrichment, which can enable the mapping of T_2* as a function of enrichment in the single spin regime. Understanding the sources of residual ^{29}Si in our films, and how to control them, is a necessary step towards targeting specific enrichments.

In order for enriched ^{28}Si to be useful as a host material for qubit spins, it must not only be isotopically pure, but chemically pure and highly crystalline so as to avoid introducing other sources of decoherence such as impurity nuclear spins and dangling bonds. Achieving single crystal epitaxial deposition of ^{28}Si films on Si(100) substrates requires elevated substrate temperatures during deposition. We previously showed that for amorphous room temperature deposition, the ^{29}Si in the film could be accounted for by $^{29}SiH_4$ incorporation into ^{28}Si films due to a physical adsorption process which was coincident with the ion beam deposition[16]. Depositing with an elevated substrate

temperature is expected to lead to a change in the activation of the ^{29}Si contamination through a chemical activation process described by a reactive sticking coefficient that is similar in nature to chemical vapor deposition (CVD). Therefore, the goal of this study is to determine how the ^{29}Si and ^{30}Si incorporation is affected by increasing the substrate deposition temperature. Measurements of residual ^{29}Si and ^{30}Si isotope fractions (amount-of-substance fraction in mol/mol, or isotopic concentration) are made using secondary ion mass spectrometry (SIMS) which is extremely sensitive to isotope ratios. This means that our monoisotopic ion beam deposition system offers a unique method of measuring the activated sticking of natural abundance SiH_4 on Si substrates because any isotopic contaminants (^{29}Si and ^{30}Si) incorporated via sticking from SiH_4 are easily distinguished from the background of pure ^{28}Si being deposited from the ion beam.

In this article, we deposit epitaxial thin films of ^{28}Si and measure the residual ^{29}Si and ^{30}Si isotopes in samples deposited in different SiH_4 partial pressures while varying the substrate deposition temperature of each sample. From these measurements, we extract the temperature dependence of the incorporation fraction, s, of $^{29}SiH_4$ due primarily to reactive sticking and determine the associated activation energy, E_c. These results give us an understanding of, and thus control over, the ^{29}Si concentration in ^{28}Si films.

II. EXPERIMENTAL METHODS

A. Ion beam system and selectivity

Enriched ^{28}Si thin films are deposited using a hyperthermal energy ion beam deposition system. This system injects commercial, natural abundance SiH_4 source gas into a high vacuum Penning-type ion source generating a Si^+ ion beam and then mass

filters the ions in a magnetic field before depositing them onto heated Si(100) substrates. The mass separation principle and ion beam system used here have been described in more detail elsewhere[16,20]. Previously, we analyzed SiH_4 incorporation in samples deposited at room temperature, but now we examine the temperature dependence of $s(T)$ at temperatures required to facilitate epitaxial growth. The SiH_4 used here is unenriched and is thus assumed to have a Si isotopic abundance roughly the same as natural Si (92.2 % ^{28}Si, 4.7 % ^{29}Si, and 3.1 % ^{30}Si). This SiH_4 is also 99.999 % pure according to the gas vendor. This SiH_4 is used to form a plasma within the ion source that both cracks and ionizes the SiH_4 molecules. From the plasma, singly charged Si^+ ions (charge of 1 e, the elementary charge) are extracted into the beamline at high voltage and enter a system of electrostatic optics, which steer them into the magnetic field of a 90° sector mass analyzer. ^{28}Si has a mass ≈ 28 u (unified atomic mass units), and by tuning to the appropriate magnetic field, ions with a mass-to-charge ratio ≈ 28 u/e (± 0.16 u/e at 28 u) pass through an aperture while those with different mass-to-charge ratios are rejected. Beyond the aperture, ions are focused onto the target substrate in an ultra-high vacuum (UHV) deposition chamber. In parallel, gas diffusion of SiH_4 from the ion source to the sample location in the deposition chamber provides the source of the ^{29}Si and ^{30}Si contamination concerning this report.

A mass spectrum of the constituents of the ion beam is generated by sweeping the magnetic field of the mass analyzer while monitoring the intensity of the ion beam current at the target. Each of the resulting series of peaks in the current vs. magnetic field signal correspond to different integer mass-to-charge ratios of atomic or molecular ions. In the mass spectrum of SiH_4, a series of mass peaks are formed starting at 28 u, which is

^{28}Si. The adjacent peak at 29 u corresponds to a combination of ^{29}Si and ^{28}SiH. We calculate the intrinsic geometric mass selectivity (i.e. mass resolution) of the ion beam system from the spectrum to estimate the amount of ^{29}Si potentially contaminating the ^{28}Si beam. These calculations use Gaussian fits to the mass peaks to determine the overlap of the 29 u peak on the 28 u peak. They give a peak separation of about 11 σ (standard deviations) and a resolving power $m/\Delta m \approx 80$ for m = 28 u, which yields a lower bound on the fraction of ions at 28 u consisting of ^{29}Si of roughly 10^{-25}, as previously discussed elsewhere[16]. However, this argument neglects gas scattering effects, which would likely be a dominant contributing factor to the contamination compared to this extremely small geometric component. Gas scattering causes an ion at mass 29 u to lose sufficient energy to be incorporated into the 28 u trajectory and pass through the selecting aperture. This scattering tail effect, or abundance selectivity, for a single magnet system can be estimated from literature to contribute ≈ 1 x 10^{-6} of the higher mass peak to the lower mass peak (for a mass of 28 u)[21–23], but it is difficult to measure experimentally in our system. That scattering fraction combined with the ^{29}Si natural abundance gives an estimate for an upper bound on the ^{29}Si concentration in the ^{28}Si beam of roughly 10^{-7}. This concentration may be significant for the samples measured in this study with the lowest ^{29}Si isotope fractions approaching 10^{-7}. However, we do not see any evidence that we are reaching this scattering enrichment limit, e.g. attenuation of the ^{30}Si isotope fractions compared to ^{29}Si, discussed further below. For the purposes of this paper, we assume the scattering tail contribution is negligible in these experiments and the ion beam is pure ^{28}Si. In this study, we consider the difference between the expected (100 %

166 enriched) and measured enrichment by identifying only the natural abundance SiH_4 gas
167 diffusing from the ion source into the deposition chamber as the source of ^{29}Si and ^{30}Si.

168 *B. Temperature and pressure determinations*

169 In order to extract the temperature dependence of the incorporation fraction, s, of
170 $^{29}SiH_4$ on $^{28}Si(100)$, a good estimate of the SiH_4 partial pressure at the sample location
171 during deposition is needed. The base pressure of the deposition chamber was measured
172 to be approximately 1.3 x 10^{-8} Pa (1 x 10^{-10} Torr) for these experiments. During operation
173 of the ion beam, SiH_4 is leaked into the ion source at a pressure of about 4 x 10^{-4} Pa (3 x
174 10^{-6} Torr), and some SiH_4 gas diffuses into the deposition chamber, which typically sees
175 a factor of 50 to 100 increase from the base pressure. We estimate the partial pressure of
176 SiH_4 at the sample from measurements of the individual gas components using a residual
177 gas analyzer (RGA) in the chamber. Typically, while operating the ion beam, the fraction
178 of total pressure increase due to SiH_4 and other Si hydrides is estimated to be about 28 %,
179 while the rest is mostly H_2. This is because a lot of SiH_4 is cracked into SiH_x, where SiH_x
180 is a combination of Si hydrides ($1 < x < 4$), and thus results in a large amount of
181 byproduct H_2. The SiH_x partial pressure is then estimated to vary from 1.4 x 10^{-7} Pa to 9.6
182 x 10^{-7} Pa (1.1 x 10^{-9} Torr to 7.2 x 10^{-9} Torr) across the high temperature samples in this
183 study. The previous room temperature samples were generally deposited in higher partial
184 pressures up to 4.4 x 10^{-5} Pa (3.3 x 10^{-7} Torr) for two samples. From the partial pressures,
185 we get an important quantity in this analysis, the SiH_x molecular gas flux, F_g, which is
186 calculated using the estimated partial pressure during deposition and the Hertz-Knudsen
187 equation,

188 $$F_g = p(2\pi m k_B T_g)^{-1/2}, \quad (1)$$

where p is the pressure, m is the mass of the gas (SiH_4), k_B is Boltzmann's constant, and T_g is the gas temperature (assumed to be 21°C). The pressures for the high temperature samples correspond to F_g gas flux values between 4 x 10^{11} $cm^{-2}s^{-1}$ and 3 x 10^{12} $cm^{-2}s^{-1}$.

The sample temperature during deposition was also carefully measured to ensure an accurate mapping of enrichment versus temperature and determination of s. Temperature was measured in this study using an infrared pyrometer that viewed the sample through a window from outside the vacuum chamber. The temperature readings were calibrated for our system by monitoring eutectic samples in the chamber near their melting temperature and adjusting the pyrometer emissivity to match the known melting point temperatures. The two temperature standards used here were a Au-Si eutectic[24] and an Al-Si eutectic, which were each held at their melting temperatures of 363 °C and 577 °C respectively while calibrating the pyrometer. Multiple calibrations are needed because the emissivity of Si is not constant with temperature. The emissivity as measured through the chamber window changes from about 0.25 at 363 °C up to 0.42 at 577 °C and is expected to reach a high value of 0.68 within the range of temperatures used in this study. This range of values is similar to emissivity values for Si surfaces reported in the literature (≈ 0.1 at 100 °C and 0.68 at > 800 °C)[25]. Including uncertainties in the calibration, the pyrometer temperature readings of the substrate are estimated to have a 5 % relative uncertainty due to fluctuations in the current used for sample heating as well as temperature gradients across the sample.

C. Substrate preparation and deposition

^{28}Si samples were deposited epitaxially on a variety of natural abundance Si(100) substrates including p-type, n-type, and undoped (intrinsic) wafers that were cleaved into

chips measuring 4 mm by 10 mm. Substrates were cleaned *ex situ* using standard Si cleaning procedures for metals and organics used in complementary metal-oxide-semiconductor (CMOS) technology consisting of a piranha etch, hydrofluoric acid (HF) strip, and "standard clean-2" (SC2)[26]. The chips are capped with a thin protective oxide during the final SC2 cleaning step. After cleaning, the chips were immediately mounted onto sample holders and loaded into the vacuum chamber via a load lock. Substrates were then prepared for deposition *in situ* by first degassing them overnight at 600 °C and then flash annealing them to 1200 °C for ≈ 10 s several times. This flash removes the oxide and produces a clean (2x1) reconstructed Si(100) surface on which to deposit ^{28}Si epitaxially. Typically, flashed substrates were inspected using a UHV scanning tunneling microscope (STM) to ensure a clean surface. The substrate temperature was then elevated to the growth temperature prior to exposure to the ion beam for deposition. To map out the ^{29}Si temperature dependence, samples were deposited at substrate temperatures ranging from 249 °C up to 812 °C in increments of roughly 100 °C. Also included in this study for qualitative comparison are data from previous amorphous samples deposited at room temperature (≈ 21 °C) on substrates that were only prepared *ex situ* with HF.

For the higher temperature samples, ^{28}Si ions were deposited onto the substrates in the hyperthermal energy regime with an average ion energy at the target of ≈ 40 eV. This energy is selected to stay as high as possible to minimize space charge effects while keeping the net sputter yield ≈ 0. Typical ion beam currents of around 500 nA were achieved over an area on the chip of about 6 mm^2, which corresponds to an average ion flux, F_i, that varied from 3 x 10^{13} cm^{-2}s^{-1} to 3 x 10^{14} cm^{-2}s^{-1}. F_i was calculated from the film thickness measured *post facto* in combination with the deposition time for each

sample. These fluxes correspond to deposition rates between 0.3 nm/min and 3.9 nm/min. The thicknesses of the deposited films were taken from the calibrations of the SIMS depth profiles and ranged from about 50 nm to over 300 nm depending on the sample and the measurement location on the deposition spot.

D. SIMS measurements

Measurements of the enrichment of the ^{28}Si films grown at different temperatures were made *ex situ* using SIMS. The samples were sputter eroded using an O_2^+ primary beam at an impact energy of 8 keV and a current of 1 nA while monitoring counts of ^{28}Si, ^{29}Si, and ^{30}Si to determine their relative abundances. The beam was focused to a probe size of a few micrometers in diameter, and it was raster-scanned over a 50 μm x 50 μm area. The analyzer's magnetic field was cycled to allow the positive secondary ions for each isotope to be detected by a secondary electron multiplier. The mass resolving power for the measurement conditions was $m/\Delta m \approx 6000$ measured at 10 % of the peak maximum. This resolving power is necessary to cleanly separate the ^{29}Si signal from the ^{28}SiH signal that arises due to the SIMS process. Under these conditions, we estimate that less than 10^{-5} of the ^{28}SiH signal contributes to the ^{29}Si measurement. Uncertainties of the isotope ratios were determined from the standard deviation of the mean of the measurements. A profilometer was used to calibrate the depth scale in the measurements, and that allowed for determination of ^{28}Si film thicknesses and growth rates.

III. ANALYTICAL APPROACH

In this study, we evaluate a multi-mechanism gas sticking deposition model to correlate the SIMS measurements of enrichment to the deposition conditions (e.g. SiH_x

partial pressure and deposition rate) for samples deposited between ≈ 21 ºC and 850 ºC. We consider two distinct sources of Si atoms that contribute to the films. The dominant (high flux) source is the ion beam, assumed to be pure ^{28}Si as discussed above, and the second is the diffusive partial pressure of SiH_x from the ion source, which contains all three Si isotopes in their natural abundance. The SIMS measurements provide the resultant isotopic concentrations for ^{29}Si or ^{30}Si as a fraction of the total Si deposited. The measured isotope fractions of ^{29}Si and ^{30}Si are modelled by the mixed ion beam deposition and gas sticking, to provide a combined deposition model, c_z (with z denoted as 29 for ^{29}Si and 30 for ^{30}Si), given by:

$$c_z = \frac{F_g a_z s}{F_g s + F_i}, \tag{2}$$

where F_g is the SiH_x gas flux, F_i is the ^{28}Si ion flux, a_z is the natural abundance of ^{29}Si or ^{30}Si in the SiH_4, and s is an effective incorporation fraction. We simplify c_z by defining the SiH_4 flux ratio $d = F_g/F_i$ that correlates the isotope concentrations to deposition conditions:

$$c_z = \frac{a_z s d}{1 + s d}, \tag{3}$$

where c_z increases approximately linearly with d in the dilute regime ($d \ll 1$) where most experiments were performed. Additionally, when $F_g \gg F_i$ (never true in our experiments), then the natural abundance source dominates and $c_z \to a_z$, the natural abundance ratio. To add statistical weight and simultaneously consider the ^{29}Si and ^{30}Si data, we generalize the isotope specific model of Eq. (3) by dividing it by each isotope's natural abundance so that ^{29}Si and ^{30}Si data can be fit together within the same model. This has the effect of changing the units from an isotope specific incorporation to total

(all isotopes) adsorbed SiH_4, which gives a total gas sticking deposition model, $c_{tot.}$, where

$$c_{tot.} = \frac{c_z}{a_z} = \frac{sd}{1 + sd}. \quad (4)$$

Eq. (4) allows us to determine the incorporation fraction s for each sample deposited at different temperatures, to get the trend of s vs. T. Additionally, since *s* represents the fraction of diffusing SiH_4 gas that become permanently incorporated in the film, at the single molecule level, *s* is the probability that a specific molecule becomes incorporated on the timescale of an arriving ion.

To describe the anticipated phenomenological behavior of s vs. T, we define a temperature dependent incorporation model, $s(T)$, that considers two classical gas incorporation mechanisms: a sticking term (physisorption), s_p, and a higher temperature reactive mechanism, s_c, (e.g., hydrogen cracking or chemisorption). Both s_c and s_p are expected to be thermally activated, where s_p decreases with increasing temperature as more molecules escape (desorb), and s_c increases with increasing temperature as more molecules react and bond to the surface. Since $c_{tot.}$ is normalized by the total flux, $s(T)$ is the probability per molecule that SiH_4 is incorporated. We define these individual components to be:

$$s_p = 1 - A_p \exp\left(-E_p/k_B T\right) \quad \text{and} \quad s_c = A_c \exp(-E_c/k_B T), \quad (5)$$

where E_p is the activation energy for "physisorption," E_c is the activation energy for "chemisorption," k_B is the Boltzmann constant, and T is the substrate temperature during deposition. The prefactors A_p and A_c are free parameters that account for the average site occupancy and the time integral over many activation attempts that occur at molecular

vibrational frequencies and other atomistic factors. From this, the total incorporation fraction at a given temperature is the sum of the two sticking components,

$$s(T) = s_p + s_c + s_0 = 1 - \mathrm{A}_p \exp\left(-E_p/k_B T\right) + A_c \exp(-E_c/k_B T) + s_0. \quad (6)$$

An s_0 term accounts for temperature independent incorporation, like activation from a collision with an ion in the depositing flux. The simple sum assumes that the two mechanisms are independent, e.g., physisorption is not a requirement for chemisorption, and that $E_c \gg E_p$ such that $s(T) \leq 1$ for all T.

IV. RESULTS AND DISCUSSION

A. ^{28}Si enrichment and pressure correlation

For all deposition temperatures (except room temperature and 249 °C), epitaxial growth of the ^{28}Si films was achieved. Interface widths of a few nanometers were found for samples grown between roughly 350 °C and 420 °C, while the surface roughness increased significantly for higher temperature samples. The sample with the best enrichment and lowest ^{29}Si isotope fractions in this study was deposited at 502 °C. A SIMS depth profile for this sample is shown in Fig. 1. Between 40 nm and 280 nm into the film, the averaged isotope fractions are; ^{28}Si: 99.9999819(35) %, ^{29}Si: 1.27(29) x 10^{-7}, and ^{30}Si: 5.5(19) x 10^{-8}. The average values for ^{29}Si and ^{30}Si are represented by dashed lines in Fig. 1 and fall below the data because of many zero counts on the SIMS detector for those measurement cycles. At a depth of around 300 nm in this sample, the sputter beam erodes into the substrate and the isotope fractions return to the natural values.

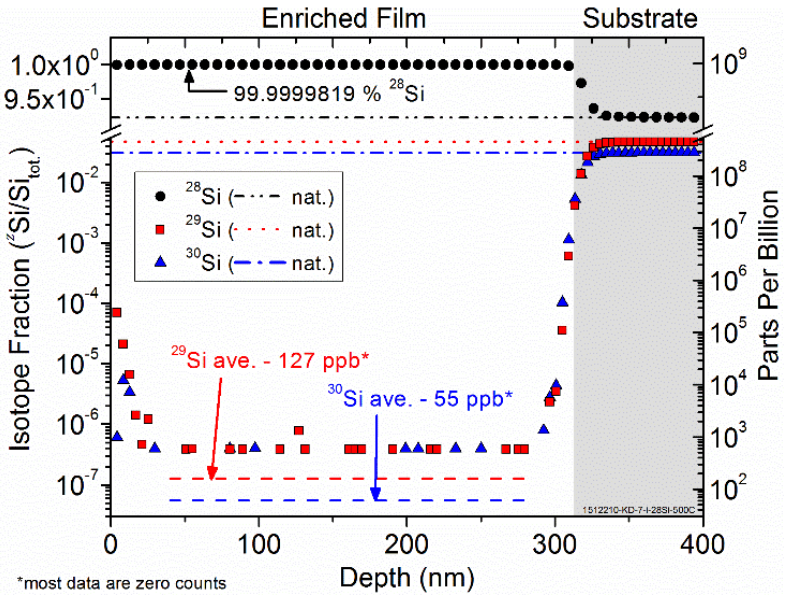

FIG. 1. (Color online) Semi-log SIMS depth profile of the 502 °C sample showing the isotope fractions of ^{28}Si (circles), ^{29}Si (squares), and ^{30}Si (triangles). The sharp increase in ^{29}Si and ^{30}Si isotope fractions to the natural abundance levels (dotted lines) at 300 nm corresponds to reaching the substrate (gray shade). The average isotope fractions (from 40 nm to 280 nm) are shown as dashed lines. These averages lie below the visible data because many of the data were zero counts.

Temperature is not the only significant experimental parameter affecting enrichment; the enrichment is also seen to depend linearly on the SiH_x partial pressure (when $F_g \ll F_i$). We plot the raw SIMS data for the room temperature samples as a function of the SiH_4 flux ratio, $d = F_g/F_i$, in Fig. 2, with ^{29}Si (squares) and ^{30}Si (triangles) isotope fractions plotted together. The top axis of Fig. 2 shows the total gas flux ratio, $F_g^{tot.}/F_i$, using the total measured pressure increase during deposition without subtracting out the estimated H_2 fraction in the gas. The hydrogen subtraction only shifts

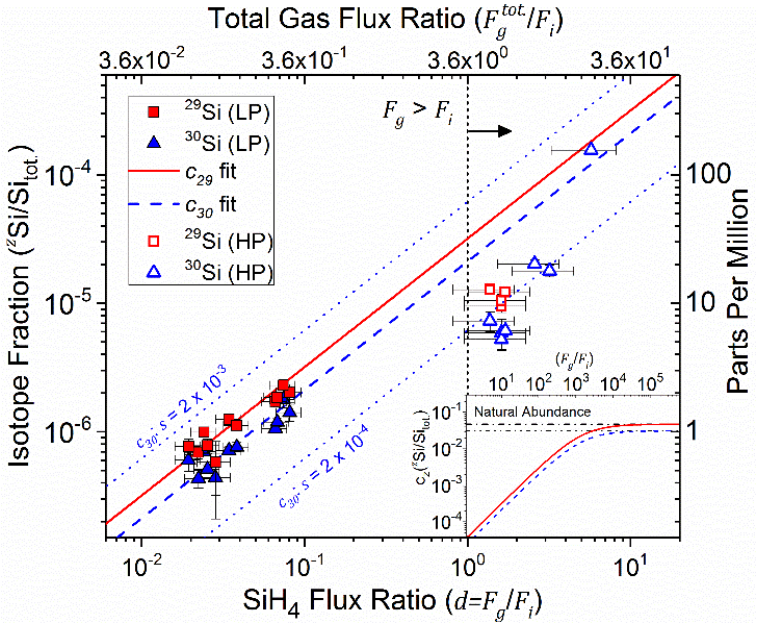

337

338 FIG. 2. (Color online) Correlation plot of isotope fraction from SIMS vs. SiH_4 flux ratio
339 $d = F_g/F_i$ shown on a log-log scale for samples deposited at room temperature (≈ 21
340 °C); ^{29}Si (squares) and ^{30}Si (triangles). The top axis is the flux ratio for the total gas flux
341 during deposition. The gas sticking deposition model, c_z is fit to the ^{29}Si and ^{30}Si data
342 (solid and dashed line respectively) and gives a value of s = 6.8(3) x 10^{-4}. c_z is linearly
343 proportional to s over the range of the data, but asymptotes (see inset) to the natural
344 abundance values when $F_g \gg F_i$ (dash-dotted lines). To demonstrate the sensitivity to
345 changes in the free parameter s, c_{30} for two other values of s (blue dotted lines) are also
346 shown. "LP" and "HP" denote data from two different experimental configurations, only
347 the "LP" data is used for quantitative analysis. Horizontal error bars are dominated by the
348 uncertainty in the pressure measurements, and vertical error bars represent the standard
349 deviation of the SIMS data.

350

351 the axis laterally and both the ^{29}Si and ^{30}Si isotope fractions have a strong linear
352 correlation with the SiH_4 flux fraction (deposition conditions), showing that a higher SiH_4
353 flux fraction produces a larger isotope fraction in the sample. This high correlation is
354 strong evidence that the diffusive SiH_x is the primary source of the minor isotopes.

To determine the probability of SiH_x being incorporated during growth, we fit the data in Fig. 2 using Eq. (3) to get c_{29} and c_{30} with s as the only free parameter. These fits are shown in Fig. 2 as solid and dashed lines respectively. They are approximately linear over the range of the data with a slope proportional to s. For $d > 10^4$, c_z asymptotes to the natural abundance values (see Fig. 2 inset) of 4.7 % for ^{29}Si and 3.1 % for ^{30}Si. The best fit to the data yields a room temperature incorporation fraction of s = 6.8(3) x 10^{-4}. The points at $d > 1$ were deposited in a different vacuum chamber with poorer pressure measurement but are included to show continuation of the qualitative trend to much higher pressures. Only the "LP" data is used for quantitative analysis at room temperature and this configuration was used for all the higher temperature work. $c_{30}(d)$ is plotted for two other values of s which span an order of magnitude around the fit value so that the reader can see the sensitivity of the fit to s. Note that when viewed as a log-log plot as in Fig. 2, c_z does not change slope as s is varied, it only changes vertical offset.

Affirmation that the diffusive SiH_4 partial pressure is the dominant source of the minor isotopes is found in the measured isotope ratios ^{29}Si/^{30}Si for each sample, shown in Fig. 3. If the minor isotope contribution originated from the ion beam, ^{30}Si would be attenuated compared to ^{29}Si and increase the ^{29}Si/^{30}Si ratio above the natural value, e.g. datum 31. Instead, the measured isotope ratios for most samples are very close to the natural value of about 1.5, indicating that the source of ^{29}Si and ^{30}Si has a natural abundance of Si isotopes, e.g., the SiH_4 source gas.

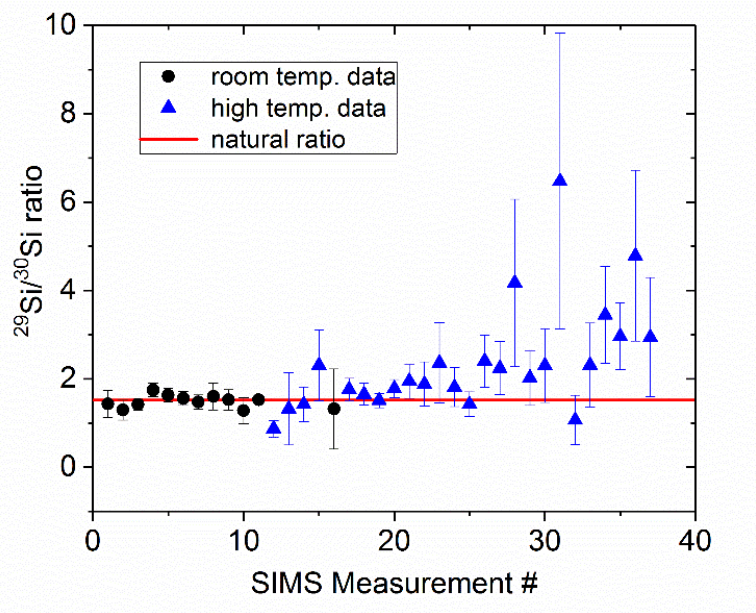

FIG. 3. (Color online) ^{29}Si/^{30}Si isotope ratios for samples deposited at room temperature (circles) and elevated temperatures (triangles). The ratios of these samples agree with the natural abundance ratio of 1.5 (line) indicating that the source of ^{29}Si and ^{30}Si is naturally abundant, probably the SiH_4 gas. Measurement numbers 28, 31, and 36, which lie above a ^{29}Si/^{30}Si ratio of four, suffer from discrete counting noise in the SIMS measurements due to a total ^{30}Si count < 10, which makes the ratio highly volatile. Error bars are derived from the standard deviation of the SIMS data.

B. Temperature dependence of ^{29}Si and s

Isotope fractions were measured by SIMS on samples grown at many different temperatures. For each SIMS measurement at each temperature, an average isotope fraction is found in the depth region where the minor isotope counts reach a minimum. The SIMS measurements from ^{28}Si samples grown at the low end of the epitaxial temperature range (249 °C) had a residual ^{29}Si isotope fraction of 7.9(12) x 10^{-7}. The sample grown at the highest temperature, 812 °C, has a ^{29}Si isotope fraction of 4.32(46) x

392 10^{-6}. This factor of five increase in isotope fraction is the focus of our analysis and
393 discussion. We note that for the samples deposited at 705 °C, 708 °C, and 812 °C,
394 significant morphological roughness may have resulted in some substrate mixing during
395 the SIMS measurement. Therefore, these data are an upper bound since the SIMS may
396 not have reached the minimum isotope fraction before breaking into the substrate. In this
397 report, we excluded data that was clearly influenced by this effect (did not reach a stable
398 isotope fraction minima), however, it is possible that this measurement artifact still
399 weakly contributed to the measured values of the isotope ratios reported here for the
400 highest temperature samples.

401 In this work, we primarily report the dependence of the ^{29}Si and ^{30}Si incorporation
402 from the SiH_4 partial pressure on the different substrate temperatures. The raw ^{29}Si
403 isotope fraction increases rapidly in the range from 502 °C (1.27 x 10^{-7}) to 812 °C (4.32 x
404 10^{-6}), however, maintaining an identical SiH_4 partial pressure and ion beam flux was not
405 possible for each sample. Using the c_z function though, we can adjust the isotope fraction
406 values at each temperature for the variations in deposition parameters. To do this, the raw
407 SIMS measurements are adjusted to a common SiH_4 flux ratio $d = F_g/F_i$. We choose the
408 d value corresponding to an area of the sample deposited at 502 °C, i.e., the lowest
409 measured isotope fractions of ^{29}Si and ^{30}Si.

410 The procedure for the adjustment is as follows: multiple values of the isotope
411 fractions are determined from SIMS plots at each temperature, e.g., Fig 1. Each SIMS
412 value is adjusted by solving Eq. (3) using the corresponding d value to determine s for
413 each datum independently, denoted as s_T^n, where n is the nth datum measured for a
414 sample deposited at temperature T. Then, using the specific s_T^n value put back into Eq

(3), we can adjust the isotope ratio to the d value of the 502 °C sample ($d_{502} = 0.0073$) and denote the adjusted value as $c_z(s_T^n, d_{502})$.

In Fig. 4, the isotope fractions adjusted for pressure and ion beam flux (deposition rate) are plotted as a function of temperature to isolate the enrichment's temperature dependence. The adjusted isotope fractions appear to initially trend downwards from ≈ 7.9 x 10^{-7} ^{29}Si at 249 °C to a minimum at the 502 °C average of about 1.3 x 10^{-7} ^{29}Si. The room temperature data appears to deviate from the low temperature trend, which is likely

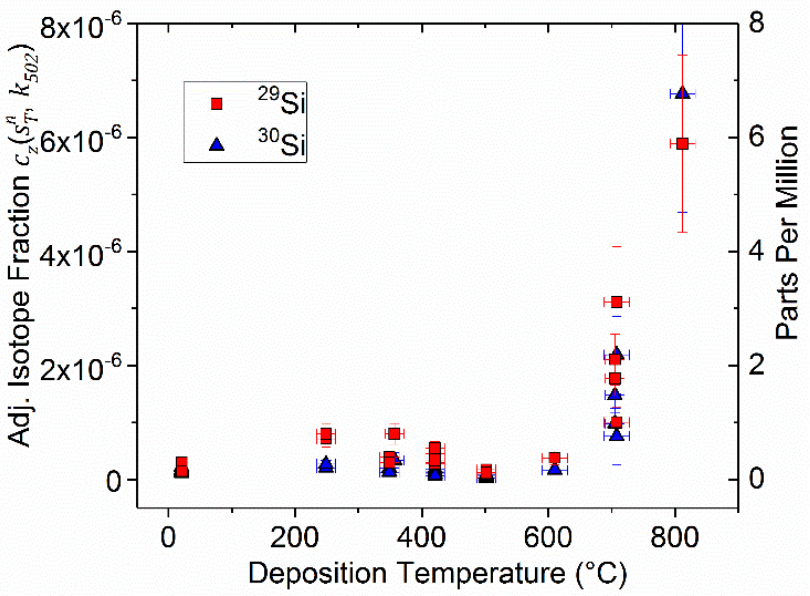

FIG. 4. (Color online) Adjusted isotope fraction, $c_z(s_T^n, d_{502})$, versus temperature for ^{29}Si (squares) and ^{30}Si (triangles). The raw isotope fractions are adjusted to the deposition conditions (F_g and F_i) of the 502 °C sample to account for differences in pressure and deposition rate amongst different samples. This shows the expected increase in isotope fraction at a given temperature for a sample deposited under the same conditions as the 502 °C sample. Horizontal error bars are due to uncertainty in the pyrometer calibration and temperature fluctuation during deposition, and vertical error bars represent the standard deviation of the SIMS data.

due to unaccounted for systematic variations, e.g., because those samples were amorphous and were grown in a different experimental configuration. Surface orientation and crystallinity are known to affect the adsorption of SiH_4 on Si surfaces[27], which may lead to a lower effective sticking coefficient compared to that of the crystalline samples. Above 502 °C, the adjusted ^{29}Si isotope fraction sharply increases up to 5.9 x 10^{-6} ^{29}Si at 812 °C. This increase is emblematic of the thermal activation of a chemical process, perhaps similar to a CVD reaction, and appears to dominate over the incorporation mechanism at lower temperatures.

We can analyze these mechanisms better by evaluating the values of s at each temperature and comparing them to the temperature dependent incorporation model. The measured isotope fractions are first converted to isotope independent SiH_4 fractions using their natural abundance values according to the generalization to obtain Eq. (4) for the total gas sticking deposition model, $c_{tot.}$. The generalized ^{29}Si and ^{30}Si data for each deposition temperature are then plotted together in Fig. 5 against their SiH_4 flux ratios and fit together using $c_{tot.}$ to get a single s_T value for each temperature.

The values of *s* determined from data (slopes of the lines in Fig. 5) are shown in Fig. 6. These incorporation fractions are a total net sticking probability; i.e., the probability that a SiH_x molecule that struck the surface was permanently incorporated into the film. The dependence of *s* on temperature closely follows the trend of the ^{29}Si and ^{30}Si isotope fractions in Fig. 4. In the lower temperature regime, s trends downwards slightly from a value of 1.6(2) x 10^{-3} at 249 °C to a minimum of 2.9(4) x 10^{-4} at 502 °C. In this temperature range, the decrease of *s* suggests reduced incorporation due to increasing thermally activated escape from physisorption (s_p) (The room temperature

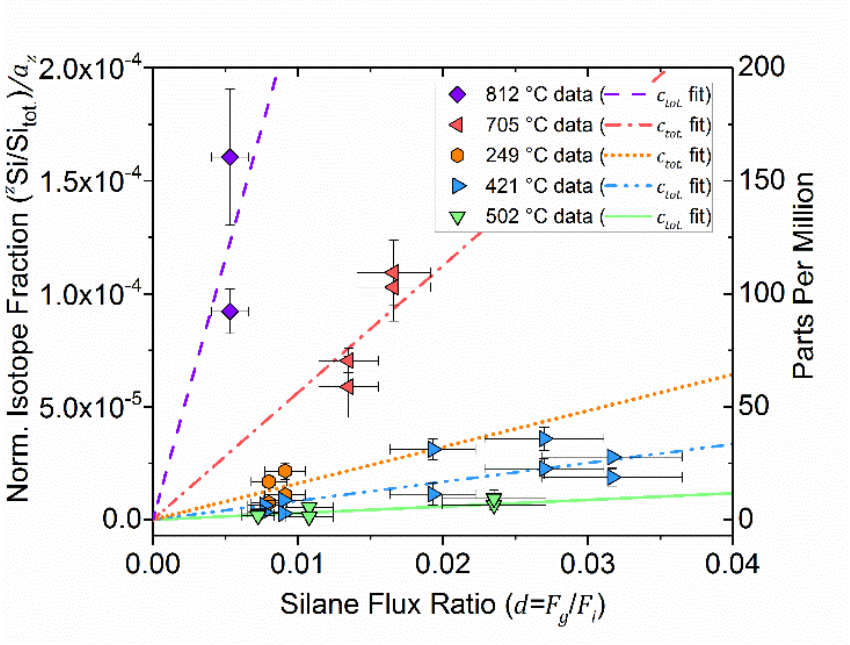

455

456 FIG. 5. (Color online) Correlation plots of the generalized isotope fractions $c_{tot.}$ vs. SiH_4
457 flux ratio shown on a linear scale for samples deposited at several elevated temperatures.
458 The raw SIMS isotope fractions for ^{29}Si and ^{30}Si are each generalized using their natural
459 abundance, a_z, to get the estimated total adsorbed SiH_4. Then c_{tot} is fit to the data for
460 each temperature (solid, dashed, dotted lines) to determine s_T. The fits originate at the
461 point (0, 0) because zero SiH_4 flux results in an adsorbed SiH_4 fraction of zero.
462 Horizontal error bars are dominated by the uncertainty in the pressure measurements, and
463 vertical error bars are derived from the standard deviation of the SIMS data.

464

465 datum is excluded since the amorphous nature of the sample will not have the same
466 adsorption kinetics). Then as T is increased above 600 °C, s rapidly increases to 2.3(5) x
467 10^{-2} at 812 °C. This increase suggests thermal activation of the reactive sticking
468 coefficient, i.e., chemisorption, s_c, which increases with increasing temperature. These
469 values of s are consistent with previously reported values of the reactive sticking
470 coefficient of silanes on Si surfaces, although there is a large variation in the literature,
471 e.g., Si CVD studies have shown the reactive sticking coefficient, s_r, to range from 5 x

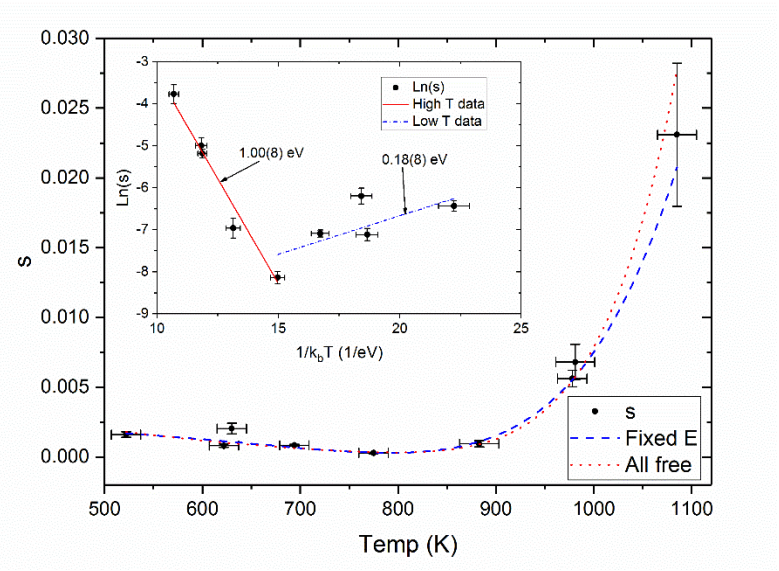

FIG. 6. (Color online) Incorporation fraction, s (circles) vs. deposition temperature. s is determined from the fits of $c_{tot.}$ to the data for each temperature in Fig 5. The fit to Eq. (6) is shown in the red dotted line with all parameters free. The inset presents the same data in Arrhenius form, ln(s) vs. $1/k_B\,T$, with linear fits to the activation energies above and below 502 °C ($1/k_B\,T \approx 15$ eV^{-1}). Using the energies determined in the inset as fixed inputs to Eq. (6), the model is refit and shown as the blue dashed line. Horizontal error bars are due to uncertainty in the pyrometer calibration and temperature fluctuation during deposition, and vertical error bars represent the standard deviation of the fit values of Fig. 5.

10^{-4} to 5 x 10^{-3} for polycrystalline Si deposition at 600 °C to 800 °C[28], and from 1 x 10^{-3} to 3 x 10^{-5} for Si(111) surfaces below 500 °C[29,30].

Next, we fit the data in Fig. 6 using the temperature dependent incorporation model of Eq. (6). This model considers physisorption (s_p) with thermally activated escape (desorption), thermally activated incorporation (s_c), e.g., due to reaction, as well as temperature independent process like ion activation (s_0). The fit to Eq. (6) while leaving all five parameters free is shown as a red dotted line in Fig. 6. Visually, this

appears to be a good fit, but several aspects of the fit parameters suggest problems, e.g., the numerical value for $E_p \approx 2 \times 10^{-4}$ eV, $s_0 \ll 0$, and several parameters have a high-degree of cross-correlation, suggesting too many degrees of freedom.

In order to break the correlations and isolate E_p and E_c, we replot the data of Fig. 6 in an Arrhenius form, $\ln(s)$ vs. $1/k_BT$ in the inset of Fig. 6. One can see two regimes of data, corresponding to above and below the 502 °C datum at $1/k_BT \approx 15$ eV^{-1}. We approximate each regime as being dominated by a distinct physical mechanism so that each segment individually can be fit to a line $\ln(s) = \ln(A) - E(1/k_BT)$ where the slope is the effective activation energy in that regime. The fit line for the higher temperature data is shown as a solid red line with a slope of 1.00 eV ± 0.08 eV while the fit to the lower temperature data is shown in a dash-dotted blue line with a slope of 0.18 eV ± 0.08 eV and have R^2 values of 0.98 and 0.61, respectively. The higher temperature value of 1.00 eV is consistent with reported activation energies for SiH_4 CVD between 600 °C and 800 °C. The literature values are found to vary between about 0.4 eV to 2.2 eV depending heavily on experimental conditions such as surface orientation, gas pressure, and hydride species[27–29,31–34].

Using the energy values determined from the slopes in the Arrhenius fits, we can input these as known values back into Eq. (6) supposing that they correspond to the energies in that model and perform the fit with fewer degrees of freedom. A plot of this fit is shown as a blue dashed line in Fig. 6. The best fit values are $s_0 = -0.9977(3)$, $A_p = 0.035(6)$, $A_c = 1023(141)$ with some correlation remaining between s_0 and A_p, but the fit yields reasonable relative errors and a $R^2 = 0.91$.

Examining the values of the best fit parameters yield some physical insights. Firstly, if we consider the zero-temperature limit (albeit a substantial extrapolation), then $s(T \to 0) = s_0 + 1 = 0.0023(6)$, as opposed to our initial assumption that $s(T \to 0) = 1$ and $s_0 \geq 0$, i.e. all the SiH_4 would be incorporated in the zero-temperature limit. The implication of needing $s_0 < 0$ to fit the data is this initial assumption is incorrect, and that adsorbing SiH_4 is not guaranteed to be incorporated. Rather, under these conditions, only ≈ 1/400 adsorbed molecules would become incorporated. Ultimately, another mechanism (besides adsorption) must be acting as a gateway to incorporation, accounting for the $s_0 + 1$ terms discussed above. We then look to possible temperature *independent* activation processes that can lead to incorporation, the most obvious being a collision from the ion beam. Focusing on the low temperature regime where we neglect (s_c), we can write a differential equation (below the activation of s_c) where

$$\frac{dn_s}{dt} = (1 - n_s)F_g - n_s \nu \exp\left(-\frac{E_p}{k_B T}\right) - p\, n_s\, F_i \,, \qquad (7)$$

with n_s being the probability a surface site is occupied, ν is the molecular vibration frequency and p corresponds to the probability that an ion collision results in the incorporation of a SiH_4 molecule. The first term is the source term from the gas flux, which becomes diminished if a substantial portion of the surface is covered by SiH_4; the second term is thermally activated desorption (similar to s_p but without the implicit integral over the gas flux rate) and the last term represents collisional activation from the ion beam. We set this equation to zero (corresponding to the steady state condition during growth) and then look at the zero temperature limit for the conditions corresponding to d_{502} at each atomic site ($F_g = 0.0013$ s^{-1}, $F_i = 0.179$ s^{-1}) and with $p = 1$. We find a

steady state occupation probability $n_s = \frac{F_g}{pF_i + F_g} = 0.0072$, and assuming all other sites would become occupied by ^{28}Si from the ion beam, then $c_{tot.} = n_s$. Considering the isotopic abundance $a_{29} = 0.047$, then the probability that a surface site is occupied by a $^{29}SiH_4$ is $n_{s-29} = 3.4 \text{ x } 10^{-4}$, and the corresponding ^{29}Si isotope ratio would also be $3.4 \text{ x } 10^{-4}$. By comparison, using the alternate $T = 0$ limit from the fit of Eq. (6) above for $s(T \to 0) = 0.0023$, and using $d_{502} = \frac{F_g}{F_i} = 0.0073$ we can extrapolate that the zero temperature concentration of silicon from the gas $c_{tot.}(\text{fit}) \approx d_{502} \cdot s(T \to 0) =$ $1.7 \text{ x } 10^{-5}$and the ^{29}Si isotope fraction would be 0.8 x 10^{-6}. These two zero temperature limits can be reconciled if we calculate $c_{tot.} = n_s \cdot p$ and drop the assumption of $p = 1$, where we use $c_{tot.} = 1.7 \text{ x } 10^{-5}$ from the Eq. (6) fit and $n_s = 0.0072$ following Eq. (7) above. From this, we find the implied ion collision activation probability $p = 0.0023$, which is numerically equal to the $s(T \to 0)$. Considering the value $p = 0.0023$, an activation probability of 1 in 400 is plausible (although probably low) for a 40 eV ion at normal incidence, but considering the uncertainties present and the extreme extrapolation to well below the limits of the data, this value should not be taken too seriously.

We do feel that the data provide good evidence for 1) a thermally activated incorporation mechanism with an activation energy of 1.00(8) eV, probably corresponding to breaking an H bond; 2) a temperature-independent activation mechanism proportional to the surface population, probably ion collisional activation; and 3) a diminishing surface population due to thermal desorption that reduces the absolute incorporation from (2).

V. SUMMARY AND CONCLUSIONS

We analyzed the measured enrichment from SIMS (i.e. residual ^{29}Si and ^{30}Si isotope fractions) of samples deposited at temperatures ranging from 249 °C to 812 °C to understand how enrichment changes as a function of temperature due to SiH_4 incorporation. From this analysis, we determined the temperature dependence of the incorporation fraction, s, and modeled it using two sticking terms. The lowest ^{29}Si isotopic concentration was found for deposition at 502 °C at 1.27(29) x 10^{-7}. A reactive incorporation mechanism due to CVD-like chemisorption is observed and increases minor isotope concentration between 502 °C up to 812 °C. While we achieve epitaxial growth for all samples deposited above 249 °C, the temperature range above 502 °C coincides with increased film roughness and crystalline defect formation, although several mechanisms are believed to contribute to this behavior. In this work, the optimal deposition temperature for minimizing the ^{29}Si isotopic concentration is found to be ≈ 500 °C, however, we consistently use 450 °C to produce high quality, smooth epitaxial films with reduced risk of chemical contamination and expect to suffer little or no decrease in enrichment.

We find an activation energy for this reactive incorporation of E_c = 1.00(8) eV. Below the activation of the reactive process, the data suggest that incorporation directly from adsorption is rare and that a temperature independent mechanism like an ion collision is likely. Understanding the role of SiH_4 gas sticking for a range of deposition temperatures is the first step in enabling production of ^{28}Si samples with targeted levels of enrichment (^{29}Si isotope fractions) facilitating a study of T_2 coherence times as a function of ^{29}Si concentration.

ACKNOWLEDGMENTS

The authors thank Aruna Ramanayaka for *ex situ* sample preparation and helpful discussions, as well as Neil Zimmerman (NIST), Michael Stewart (NIST), Vlad Oleshko (NIST), Rick Silver (NIST), Kai Li (NIST), Pradeep Namboodiri (NIST), and Shin Muramoto (NIST) for other contributions and helpful discussions.

[1] M. Steger, K. Saeedi, M.L.W. Thewalt, J.J.L. Morton, H. Riemann, N. V Abrosimov, P. Becker, and H.J. Pohl, Science (80-.). **336**, 1280 (2012).

[2] W.M. Witzel, M.S. Carroll, Ł. Cywiński, and S. Das Sarma, Phys. Rev. B **86**, 35452 (2012).

[3] E. Abe, A.M. Tyryshkin, S. Tojo, J.J.L. Morton, W.M. Witzel, A. Fujimoto, J.W. Ager, E.E. Haller, J. Isoya, S.A. Lyon, M.L.W. Thewalt, and K.M. Itoh, Phys. Rev. B **82**, (2010).

[4] J.T. Muhonen, J.P. Dehollain, A. Laucht, F.E. Hudson, R. Kalra, T. Sekiguchi, K.M. Itoh, D.N. Jamieson, J.C. McCallum, A.S. Dzurak, and A. Morello, Nat Nano **9**, 986 (2014).

[5] A.M. Tyryshkin, S. Tojo, J.J.L. Morton, H. Riemann, N. V Abrosimov, P. Becker, H.-J. Pohl, T. Schenkel, M.L.W. Thewalt, K.M. Itoh, and S.A. Lyon, Nat. Mater. **11**, 143 (2012).

[6] K. Saeedi, S. Simmons, J.Z. Salvail, P. Dluhy, H. Riemann, N. V Abrosimov, P. Becker, H.-J. Pohl, J.J.L. Morton, and M.L.W. Thewalt, Science (80-.). **342**, 830 (2013).

[7] F.A. Zwanenburg, A.S. Dzurak, A. Morello, M.Y. Simmons, L.C.L. Hollenberg, G.

602 Klimeck, S. Rogge, S.N. Coppersmith, and M.A. Eriksson, Rev. Mod. Phys. **85**, 961
603 (2013).

604 [8] A. Wild, J. Kierig, J. Sailer, J.W. Ager, E.E. Haller, G. Abstreiter, S. Ludwig, and D.
605 Bougeard, Appl. Phys. Lett. **100**, (2012).

606 [9] J.J.L. Morton, A.M. Tyryshkin, R.M. Brown, S. Shankar, B.W. Lovett, A. Ardavan, T.
607 Schenkel, E.E. Haller, J.W. Ager, and S.A. Lyon, Nature **455**, 1085 (2008).

608 [10] L.A. Tracy, D.R. Luhman, S.M. Carr, N.C. Bishop, G.A. Ten Eyck, T. Pluym, J.R.
609 Wendt, M.P. Lilly, and M.S. Carroll, Appl. Phys. Lett. **108**, 63101 (2016).

610 [11] VeldhorstM, J.C.C. Hwang, C.H. Yang, A.W. Leenstra, B. de Ronde, J.P. Dehollain,
611 J.T. Muhonen, F.E. Hudson, K.M. Itoh, MorelloA, and A.S. Dzurak, Nat Nano **9**, 981
612 (2014).

613 [12] M.L.W. Thewalt, A. Yang, M. Steger, D. Karaiskaj, M. Cardona, H. Riemann, N. V.
614 Abrosimov, A. V. Gusev, A.D. Bulanov, I.D. Kovalev, A.K. Kaliteevskii, O.N. Godisov,
615 P. Becker, H.J. Pohl, E.E. Haller, J.W. Ager, and K.M. Itoh, J. Appl. Phys. **101**, 81724
616 (2007).

617 [13] P. Becker, H.J. Pohl, H. Riemann, and N. Abrosimov, Phys. Status Solidi a-
618 Applications Mater. Sci. **207**, 49 (2010).

619 [14] K.M. Itoh and H. Watanabe, MRS Commun. **4**, 143 (2014).

620 [15] K.J. Dwyer, J.M. Pomeroy, and D.S. Simons, Appl. Phys. Lett. **102**, (2013).

621 [16] K.J. Dwyer, J.M. Pomeroy, D.S. Simons, K.L. Steffens, and J.W. Lau, J. Phys. D.
622 Appl. Phys. **47**, 345105 (2014).

[17] N. Tsubouchi, A. Chayahara, Y. Mokuno, A. Kinomura, and Y. Horino, Japanese J. Appl. Phys. Part 2-Letters **40**, L1283 (2001).

[18] A.H. Albayati, K.J. Boyd, D. Marton, S.S. Todorov, J.W. Rabalais, Z.H. Zhang, and W.K. Chu, J. Appl. Phys. **76**, 4383 (1994).

[19] J.W. Rabalais, A.H. Al-Bayati, K.J. Boyd, D. Marton, J. Kulik, Z. Zhang, and W.K. Chu, Phys. Rev. B **53**, 10781 (1996).

[20] J.M. Pomeroy, A.J. Couture, M.V.R. Murty, E.N. Butler, and B.H. Cooper, Rev. Sci. Instrum. **73**, 3846 (2002).

[21] F.G. Ruedenauer, Rev. Sci. Instrum. **41**, 1487 (1970).

[22] N.J. Freeman, N.R. Daly, and R.E. Powell, Rev. Sci. Instrum. **38**, 945 (1967).

[23] T.R. Ireland, Rev. Sci. Instrum. **84**, 11101 (2013).

[24] C.Y. Kuo and C. Gau, Thin Solid Films **519**, 3603 (2011).

[25] V.I. Rudakov, V. V. Ovcharov, and V.P. Prigara, Russ. Microelectron. **41**, 15 (2012).

[26] W. Kern, *Handbook of Semiconductor Wafer Cleaning Technology: Science, Technology, and Applications* (Noyes Publications, 1993).

[27] J.H. Comfort and R. Reif, J. Electrochem. Soc. **136**, 2386 (1989).

[28] R.J. Buss, P. Ho, W.G. Breiland, and M.E. Coltrin, J. Appl. Phys. **63**, 2808 (1988).

[29] S.M. Gates, C.M. Greenlief, D.B. Beach, and R.R. Kunz, Chem. Phys. Lett. **154**, 505 (1989).

[30] S.M. Gates, Surf. Sci. **195**, 307 (1988).

643 [31] B.A. Scott, R.D. Estes, and J.M. Jasinski, J. Chem. Phys. **89**, 2544 (1988).

644 [32] K.F. Roenigk, K.F. Jensen, and R.W. Carr, J. Phys. Chem. **91**, 5732 (1987).

645 [33] F. Hirose, J. Cryst. Growth **179**, 108 (1997).

646 [34] S.M. Gates, C.M. Greenlief, S.K. Kulkarni, and H.H. Sawin, J. Vac. Sci. Technol. A

647 Vacuum, Surfaces, Film. **8**, 2965 (1990).

648